First-principles study of spin-disorder resistivity of heavy rare-earth metals: Gd–Tm series

J. K. Glasbrenner and K. D. Belashchenko
Department of Physics and Astronomy and Nebraska Center for Materials and Nanoscience, University of Nebraska–Lincoln, Lincoln, Nebraska 68588, USA

J. Kudrnovský and V. Drchal
Institute of Physics, Academy of Sciences of the Czech Republic, CZ-182 21 Praha 8, Czech Republic

S. Khmelevskyi
CMS, Institute of Applied Physics, Vienna University of Technology, Gußhausstrasse 25a, Makartvilla, A-1020 Vienna, Austria

I. Turek
Institute of Physics of Materials, Academy of Sciences of the Czech Republic, Žižkova 22, CZ-616 62 Brno, Czech Republic
(Received 8 May 2012; published 7 June 2012)

Electrical resistivity of heavy rare-earth metals has a dominant contribution from thermal spin-disorder scattering. Here this spin-disorder resistivity is calculated for the Gd-Tm series of metals in the paramagnetic state. Calculations are performed within the tight-binding linear muffin-tin orbital method using two complementary methods: (1) averaging of the Landauer-Büttiker conductance of a supercell over random noncollinear spin-disorder configurations, and (2) linear response calculations with the spin-disordered state described in the coherent potential approximation. The agreement between these two methods is found to be excellent. The spin-disorder resistivity in the series follows an almost universal dependence on the exchange splitting. While the crystallographic anisotropy of the spin-disorder resistivity agrees well with experiment, its magnitude is significantly underestimated. These results suggest that the classical picture of slowly rotating self-consistent local moments is inadequate for rare-earth metals. A simple quantum correction improves agreement with experiment but does not fully account for the discrepancy, suggesting that more complicated scattering mechanisms may be important.

DOI: 10.1103/PhysRevB.85.214405 PACS number(s): 72.15.Eb, 75.47.−m, 71.20.Eh

I. INTRODUCTION

Scattering on spin fluctuations in magnetic metals adds an "anomalous" contribution to the electrical resistivity.[1–3] Contrary to other scattering mechanisms, such as impurity and phonon ones, this spin-disorder scattering is not well understood because the theory of spin fluctuations at elevated temperatures is far from being complete.[4] The minimal model of spin-disorder resistivity (SDR) is based on the s-d (or d-f) Hamiltonian, containing on-site interaction of the conduction electrons with spins localized on lattice sites, which are subject to thermal fluctuations.[5–7] This interaction is also responsible for the indirect exchange coupling described by the Ruderman-Kittel-Kasuya-Yosida (RKKY) theory.[8,9] Extensions of this model to include Fermi-surface anisotropy and the appearance of "superzones" (in the helically ordered state) in the heavy rare-earth materials have also been proposed.[8–13]

First-principles calculations of SDR provide an opportunity to test the models of spin disorder quantitatively by comparing the predicted SDR with experiment. In particular, such a study of spin-disorder resistivity of Fe and Ni (Ref. 14) suggests that the spin fluctuations in these materials are described reasonably well by slowly rotating, classical local magnetic moments, supporting the widely used "adiabatic" model of spin fluctuations.[15]

The series of heavy rare-earth metals (Gd-Tm) provides an interesting case study because the $4f$ electrons supplying most of the local moment are much more localized compared to the transition metals, while the orbitals moments are not quenched. It may therefore be inadequate to treat the spin fluctuations in rare-earth metals as classical spin rotations. Systematic experimental studies of the electrical properties of heavy rare-earth metals were carried out by Legvold *et al*. These included polycrystalline[16,17] and single-crystal samples,[18–23] allowing a compilation of the SDR in the in-plane and c-axis directions of the hexagonal crystal structure. Single-crystal resistivity measurements have also been performed by other groups.[24–28]

In the f-d model picture, the assumption that the $4f$ local moment can be treated as a quantum multiplet with a fixed angular momentum J leads to the SDR being proportional to $J(J+1)$ in the paramagnetic state (in the Born approximation). The effective scattering potential is, however, provided largely by spin alone. Therefore, in this picture, the SDR in the Gd-Tm series should behave as $S^2(J+1)/J$. This picture appears to agree reasonably well with experimental data,[10,29] but only after an empirical electronic correction is included.[10]

The choice of the angular momentum J for the quantum multiplet[10,29] is based on the assumption that spin-orbit coupling is sufficiently strong to enforce the collinearity of **S** and **L** at all times. If spin-orbit coupling is small compared to other relevant energy scales, then the role of J should be played by S, and SDR should behave as $S(S+1)$ in the Gd-Tm series. However, band structure calculations[30] show that the $4f$ bandwidth is comparable to or greater than the spin-orbit splittings of the localized $4f$ multiplets with different J

values, which are on the order of 0.1 eV. The local exchange potential acting on the conduction electrons by the fluctuating $4f$ moments is on the order of 1 eV in Gd and decreases linearly with the $4f$ spin moment later in the series. This fluctuating exchange potential should induce an uncertainty of the conduction electron energy on the order of a few tenths of an electron volt. Therefore, the assumption that the J value of the fluctuating $4f$ shell should be conserved in the scattering process is not well justified. Since all of the relevant energy scales (spin-orbit splittings, exchange splitting, bandwidth) are of the same order of magnitude, the effect of spin and orbital momentum quantization on SDR may be quite complicated.

In this paper, we study the SDR for the Gd-Tm series using first-principles calculations based on density functional theory. We use two complementary approaches, one using supercell averaging of the Landauer-Büttiker conductance, and the other based on linear response calculations applied to the paramagnetic state described within the coherent potential approximation. In most calculations, the $4f$ electrons are treated as fully localized, but the effect of including them in the valence basis is also considered. The results of our calculations represent the predictions of the classical spin model. Contrary to the case of transition metals,[14] our results for Gd-Tm are systematically and significantly lower compared to experimental data, suggesting that the quantum character of the $4f$ shell is indeed important. However, we found that neither a $(J+1)/J$ nor an $(S+1)/S$ correction brings the results in close agreement with experiment, supporting the qualitative argument that the fluctuations of the $4f$ shell are not well described either by the fixed-J model or by the assumption that **S** and **L** are weakly coupled.

II. COMPUTATIONAL METHODS

The $4f$ electrons in rare-earth materials are strongly localized and obey Hund's rules, producing large local magnetic moments. These electrons are not well described by the local-density approximation (LDA),[30] which places the $4f$ energy bands close to the Fermi level in disagreement with photoemission experiments.[31] This problem can be addressed in two ways. First, one can use the LDA + U method for the $4f$ electrons, which introduces a correlation gap and removes the $4f$ states from the Fermi level. The second way is to treat the $4f$ orbitals as fully localized by excluding them from the valence basis and filling them in accordance with Hund's rules (the "open-core" approximation). In both cases, the partially filled $4f$ states supply local moments and contribute to the scattering (exchange) potential. In the open-core approach, they are explicitly prevented from carrying current; in the LDA + U approach, their contribution to the current is expected to be small, but they can still affect the scattering rates by modifying the final states. Both solutions produce similar band structures near the Fermi level,[30] and therefore they can be expected to produce similar results for transport.

Our calculations of SDR are based on the tight-binding linear muffin-tin orbital (TB-LMTO) method.[32] In most of our calculations, we used the open-core approximation[33] for the $4f$ states, but we have also considered the effect of including the $4f$ states in the valence basis. As expected, this inclusion increases the resistivity by a small amount.

We used two approaches for SDR calculations, namely, the Landauer-Büttiker (LB) method and the linear response technique applied within the disordered local-moment (DLM) model. In all calculations, we consider the paramagnetic state to be a completely random, uncorrelated distribution of local-moment directions on different atomic sites. The results are compared with experimental data, from which the phonon and impurity contributions have been removed by an appropriate fitting.

While the LB approach can be used for more complicated spin statistics,[14] the DLM method is, by design, appropriate only to uncorrelated spin disorder due to its reliance on the single-site approximation. The DLM method uses the bulk geometry and computes the resistivity by a reciprocal-space integration of the Kubo-Greenwood formula, while the LB approach requires the construction of supercells.

A. Landauer-Büttiker approach

The method used for SDR calculations was described in Ref. 14. All heavy rare-earth elements examined in this study (Gd, Tb, Dy, Ho, Er, and Tm) have a hexagonal close-packed crystal structure. The resistivity tensor has two independent components for current flowing parallel and perpendicular to the hexagonal c axis. For transport along the c axis, we used supercells with a 4×4 cross section (16 atoms per monolayer, interlayer spacing $c/2$) of area $8a^2\sqrt{3}$. The in-plane SDR was calculated for the current flowing parallel to one of the in-plane lattice vectors. For this direction, we used supercells with a 3×2 (12 atoms per monolayer, interlayer spacing a) rectangular cross section of width $3a\sqrt{3}$ and height $2c$. The integration of the conductance over the two-dimensional Brillouin zone is performed using a 24×24 k-point mesh for both transport directions, and the result is averaged over 15 random noncollinear spin distributions. For a convergence test, see Appendix A.

Figure 1 shows the configurationally averaged area-resistance product RA as a function of the thickness L of the active disordered region in our supercell calculations for Gd, Tb, and Tm for both transport directions. The plots for the other three elements (Dy, Ho, and Er) are similar. The ohmic regime is quickly reached for all elements. The SDR is obtained from the slope of the fit to the linear region.

To check the validity of the open-core approximation for transport calculations, we include the $4f$ orbitals in the valence basis set and calculate the self-consistent potentials using the fully localized limit of LDA + U (Ref. 34) applied to the $4f$ electrons. The population of the $4f$ states is specified manually by a diagonal density matrix in the spherical harmonic representation (which is not subject to self-consistency); the orbitals are filled according to Hund's rules. For Gd, we used $U = 6.7$ eV and $J = 0.7$ eV. The band structure agrees with Ref. 30 with the unoccupied $4f$ states located 2 eV above the Fermi energy. For Ho, we fixed $J = 0.7$ eV and adjusted the U parameter to $U = 8.0$ eV to place the minority-spin $4f$ bands at 2 eV above the Fermi level, according to the photoemission data.[31] For the transport calculation, we then use the (less expensive) Ising approximation by randomly assigning "up" and "down" directions for the local moments. (This approximation is justified by good agreement with DLM

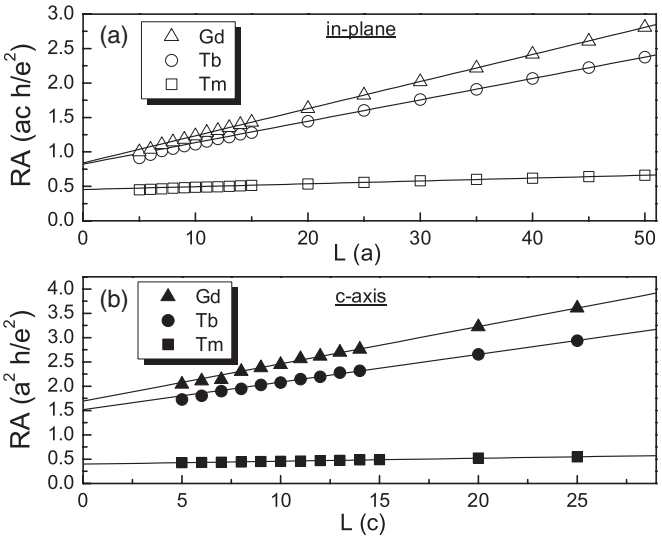

FIG. 1. Area-resistance product RA vs the thickness L of the disordered region for both transport directions for Gd, Tb, and Tm (LB method). Each point corresponds to an average of 15 or more random spin-disorder configurations. (a) In-plane direction, open shapes; (b) c-axis direction, closed shapes. Triangles: Gd; circles: Tb; squares: Tm.

results in all other cases.) The orbital occupations are also adjusted so that the orbital moments are parallel to spin moments on all sites.

B. Disordered local-moment (DLM) model

The DLM approach[15] describes the paramagnetic state above the Curie point, approximating it as an ensemble of randomly oriented local magnetic moments. The electronic structure of this state is evaluated self-consistently using the coherent potential approximation (CPA). The solution for the spherically symmetric vector model is conveniently equivalent to that for the fictitious equiconcentrational binary alloy, whose two components represent atoms with antiparallel local moments. The spin-disorder part of the total resistivity can then be associated with the "residual" resistivity of the DLM state viewed as a binary alloy, which is calculated within the Kubo-Greenwood approach (strict justification of the validity of this calculation will be presented elsewhere). An implementation of the DLM method for resistivity studies was done in Ref. 35. Our implementation of the linear response technique within the TB-LMTO-CPA method, including disorder-induced vertex corrections, is described in Refs. 36 and 37.

As a test case, we calculated the SDR for bcc iron using the DLM method and the *spd* basis. The resistivity is 85 $\mu\Omega$ cm, which agrees well both with supercell LB calculations[14] and with experiment, while the value obtained in Ref. 35 is almost two times larger. The origin of this disagreement is unclear. The method of Ref. 35 utilizes a hybrid method where the electronic structure is described by the DLM method, but the resistivity is found from the slope in the multilayer geometry as a limit from large imaginary parts of the energy (1 and 2 mRy). This method also neglects vertex corrections, thus violating current conservation.

III. REVIEW OF EXPERIMENTAL DATA

The experimental data in Table I are those of Legvold and coworkers[17–23] and those of other groups.[24,26–28] The former set of SDR values for Gd, Tb, Dy, Ho, and Er are taken from the compilation plot in Ref. 10 and agree well with our own fits to the single-crystal resistivity data. The in-plane and c-axis SDRs for Tm are explicitly reported in Ref. 23, as are the single-crystal data for Gd by Maezawa *et al.*[26] and for Er (Ref. 28) and Tm (Ref. 27) by Ellerby *et al.* The additional

TABLE I. SDR of heavy rare-earth metals calculated using the Landauer-Büttiker (LB) and disordered local-moment (DLM) methods. First (second) row for each element: Atomic potentials taken from the ferromagnetic state (from self-consistent DLM local moments). Experimental data are from Refs. 17–23 or as cited.

	Lattice parameters	Moment	In-plane SDR ($\mu\Omega$ cm)			c-axis SDR ($\mu\Omega$ cm)			Polycrystal SDR ($\mu\Omega$ cm)		
Element	(a.u.)	(μ_B)	LB	DLM	Expt.	LB	DLM	Expt.	LB	DLM	Expt.
Gd	$a = 6.858$	7.72	58.9	59.1	108, 105[a]	44.9	41.5	96, 95[a]	54.2	53.2	106.4
	$c = 10.952$	7.44	42.0	40.2		31.3	26.9		38.4	35.7	
Tb	$a = 6.805$	6.64	45.6	46.0	82	33.5	30.2	66	41.6	40.7	85.7
	$c = 10.759$	6.35	29.1	27.7		22.2	17.6		26.8	24.3	
Dy	$a = 6.784$	5.58	35.4	35.3	62, 57[b]	25.1	22.6	44, 45[b]	32.0	31.1	57.6
	$c = 10.651$	5.27	19.4	18.6		14.1	11.7		17.6	16.3	
Ho	$a = 6.760$	4.46	23.8	22.8	41	16.8	14.3	24	21.5	20.0	32.3
	$c = 10.612$	4.20	12.0	10.8		7.93	6.8		10.6	9.43	
Er	$a = 6.725$	3.33	13.4	12.2	21, 32.4[c]	8.56	7.5	13, 18.0[c]	11.8	10.6	23.6
	$c = 10.559$	3.14	6.68	5.94		4.11	3.44		5.82	4.81	
Tm	$a = 6.685$	2.21	5.96	5.23	22.3, 21.2[d]	3.43	3.2	7.4, 9.0[d]	5.12	4.56	14.9
	$c = 10.497$	2.088	3.00	2.32		1.67	1.44		2.56	2.02	

[a]Reference 26.
[b]Reference 24.
[c]Reference 28.
[d]Reference 27.

values for Dy are obtained from the plots of Ref. 24 by an appropriate fitting.

For Gd and Dy, the resistivity curves and SDR values reported by different references agree quite well. For Er and Tm, the resistivity curves from different measurements are similar in shape and indicate the same transition temperatures, but the absolute values of the residual-subtracted resistivities differ. For Er, the residual-subtracted resistivities reported by Ellerby *et al*. are systematically larger compared to the results of Legvold *et al*. For example, the resistivity at the Néel temperature, $T_N = 85$K, is about 6 $\mu\Omega$ cm larger in the c-axis direction and about 19 $\mu\Omega$ cm larger in the in-plane direction. The SDRs do not agree either, with SDRs from Ellerby *et al*. being a factor of 1.4 to 1.5 larger. For Tm, the disagreement is in the opposite direction; Ellerby *et al*. note that their c-axis (in-plane) resistivity curves are a factor of 2 (factor of 1.3) smaller compared to Legvold *et al*. The SDRs in the two studies, however, are in agreement.

The source of these disagreements is currently unknown. Ellerby *et al*. mentioned[27] that the discrepancy might be due to errors in determining the cross-sectional areas of the samples. Another problem may be the purity of the samples. The residual resistivities reported by Legvold *et al*. for Er are rather large and of the same order as the SDRs. In the rest of the heavy rare-earth experiments by Legvold *et al*., the residual resistivities are between 3 and 6 $\mu\Omega$ cm. These discrepancies introduce some ambiguity, at least in the case of Er, when comparing the calculated SDR with experiment.

IV. RESULTS

For each element and transport direction, we performed two sets of calculations corresponding to different atomic potentials. The first set of calculations used self-consistent potentials from the collinear ferromagnetic ground state of each metal. These results are listed in the first row for each element in Table I. The second set used potentials with reduced local moments taken from the self-consistent DLM calculations for the paramagnetic state. These results are listed in the second row for each element. To compare the effect of local-moment reduction in both methods, the atomic potentials are calculated self-consistently in the presence of an appropriately adjusted external field, constraining the local moments to their DLM values. These atomic potentials are then used in the LB calculations. We refer to these as the fixed-spin moment (FSM) calculations.

In order to compare the band structure obtained using the DLM method with explicit supercell calculations (to which DLM is an approximation), we constructed 64-atom supercells for Gd (4 hexagonal monolayers with 16 atoms per monolayer, periodically repeated in three dimensions). We used FSM potentials as input and generated seven different spin-disorder configurations by randomly assigning the directions of all local moments in the supercell. Then the partial density of states (DOS) for each site was calculated in the local reference frame (z axis collinear with local-moment direction) and then averaged over all sites and all seven configurations. At the same time, the output local moments were also calculated and averaged. This average output moment was 7.46 μ_B with a standard deviation of 0.03 μ_B, comparing well with the input moment of 7.44 μ_B. The averaged local DOS shown in Fig. 2 is almost indistinguishable from the self-consistent DLM result of Ref. 38. This agreement shows that the DLM method provides an accurate description of the band structure of rare-earth metals. This agreement extends to transport calculations, as discussed below.

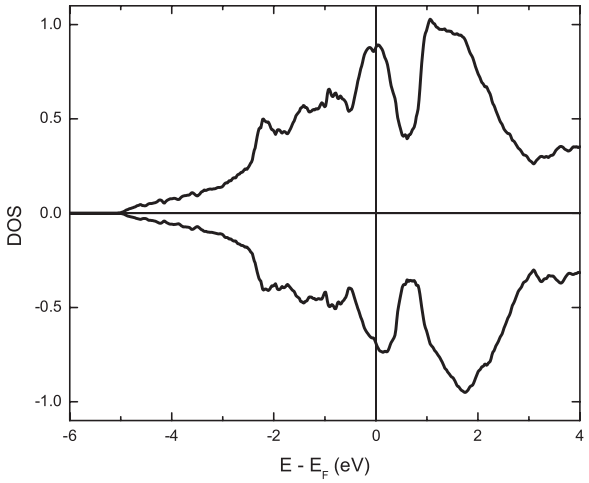

FIG. 2. Spin-projected local DOS of paramagnetic Gd averaged over 64-atom supercells with random noncollinear local-moment orientations. The valence basis includes s, p, and d states, while the fully spin-polarized $4f$ shell is included in the open-core approximation. The total (input) local moment is 7.44 μ_B. (Note the excellent agreement with the DLM result of Ref. 38.)

Table I lists the SDR results obtained using both the LB and DLM methods. The SDR for a polycrystal was estimated using the empirical formula[39]

$$\rho_{\text{poly}} = \tfrac{1}{3}(2\rho_{\perp} + \rho_{\parallel}). \quad (1)$$

The overall trend in the Gd-Tm series is represented by Fig. 3, where the LB results are plotted as a function of the square of the exchange splitting Δ. The graphs include the results obtained using both ferromagnetic and FSM input potentials listed in Table I. We also show the c-axis SDR in Gd calculated using several other values of the local moment constrained by FSM. The exchange splitting Δ is defined as the difference between the majority- and minority-spin $5d$ band centers (LMTO C parameters) obtained from the LMTO parametrization of the (third-order) potential function $P(E)$.[40] To improve the accuracy of this determination, these parametrizations are performed with the LMTO linearization energies ϵ_ν for both spins selected so that they are close to the C parameter for the same spin.

Calculated SDR for Gd and Ho with the $4f$ orbitals treated using the LDA + U method are also shown in Fig. 3. LDA + U calculations enhance the local moments compared to the open-core approximation to 7.87 μ_B for Gd and 4.64 μ_B for Ho. The calculated SDR are also enhanced to 81.7 $\mu\Omega$ cm (in-plane) and 68.2 $\mu\Omega$ cm (c-axis) for Gd, and to 44.4 $\mu\Omega$ cm (in-plane) and 31.6 $\mu\Omega$ cm (c-axis) for Ho.

As seen from Table I, the calculated results are systematically and significantly lower compared to experimental data, particularly when DLM local moments are used. Figure 4 shows the effect of applying quantum corrections according

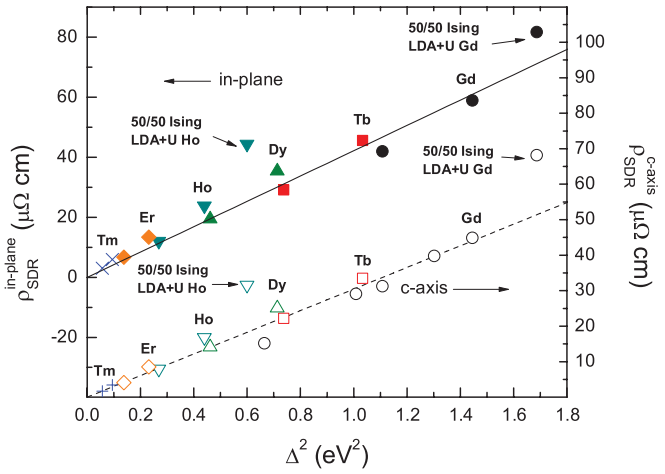

FIG. 3. (Color online) SDR as a function of the squared exchange splitting Δ^2 in the open-core approximation (or as indicated). Filled shapes: in-plane SDR; open shapes: c-axis SDR. Circles: Gd; squares: Tb; triangles: Dy; inverted triangles: Ho; diamonds: Er; crosses: in-plane Tm; pluses: c-axis Tm. Points labeled 50/50 Ising LDA + U: calculations with LDA + U for $4f$ orbitals in the basis set and Ising spin disorder.

to the models mentioned in Sec. I. For this purpose, we used the LB results obtained using the atomic potential from the ferromagnetic state, which are somewhat closer to experiment. The experimental data are plotted for comparison.

V. DISCUSSION

Table I demonstrates excellent agreement between the LB and DLM methods. Since the DLM method may be viewed as a single-site approximation to LB results, this agreement shows that the DLM method is quite accurate for transport calculations in all of the heavy rare-earth metals. This is not surprising in view of the excellent agreement of the DOS demonstrated above.

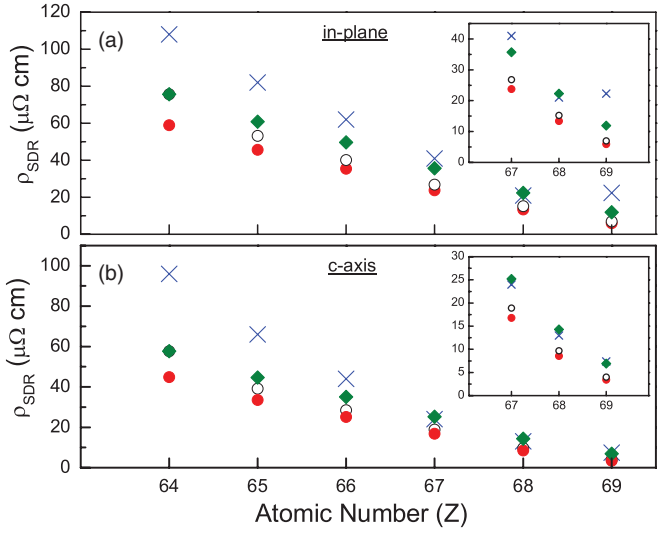

FIG. 4. (Color online) Comparison of calculated SDR with experiment and the effect of quantum corrections. (a) In-plane direction, (b) c-axis direction. Insets: enlarged scale. Crosses: experimental data (Legvold *et al.*); filled circles: LB calculations with atomic potentials taken from the ferromagnetic state. Filled diamonds: LB results multiplied by $(S+1)/S$; open circles: LB results multiplied by $(J+1)/J$.

The dependence of SDR on Δ^2 shown in Fig. 3 indicates a fairly universal linear trend for both crystallographic directions of transport. Since the exchange splitting plays the role of the disorder strength for SDR, this approximately linear dependence is natural. Still, Fig. 3 also reveals systematic deviations from this general trend. The $\rho(\Delta^2)$ dependencies for individual elements (obtained using FSM) tend to have a larger slope compared to the universal $\rho \propto \Delta^2$ trend for the series. In particular, when two different elements are constrained by FSM to have the same exchange splitting Δ, the heavier element has a somewhat larger SDR for both crystallographic directions (compare the nearby points for Dy and Tb, or those for Ho and Dy). These deviations can at least partially be related to the systematic reduction of the Fermi velocities in the series. Table II lists the values of the Fermi-surface integral, which appears in the semiclassical expression for the conductivity in the τ approximation. Note, however, that a direct application of the semiclassical theory to the SDR problem would be rather questionable. Indeed, such treatment requires that the electronic bands are well defined, and that the typical separations between them are small compared to the scattering potential. In the SDR problem, the bands are spin degenerate in the absence of the scattering potential; in the paramagnetic state, the band splitting and the scattering potential are of the same order.

The calculated in-plane resistivity is greater compared to the c-axis direction for all elements, and the magnitude of this anisotropy gradually increases in the Gd-Tm series. These features agree very well with the experimental data, suggesting that first-principles calculations correctly capture the anisotropy of the electronic structure near the Fermi surface and its dependence on the local moment of the $4f$ shell. Note that the anisotropy of SDR is much smaller than that of the Fermi-surface integral for σ in the τ approximation (see Table II); this latter anisotropy, moreover, barely depends on the nuclear charge.

Contrary to the crystallographic anisotropy of SDR and its trend in the series, the magnitude of the calculated SDR is significantly smaller compared to experiment, even when the atomic potentials from the ferromagnetic state are used (see Table I and Fig. 4). The experimental values are larger by factors of 1.83 (2.14) in-plane (c-axis) for Gd, 1.80 (1.97) for Tb, 1.75 (1.75) for Dy, 1.72 (1.43) for Ho, 1.57 (1.52) for

TABLE II. Calculated integrals $\int v_\alpha^2 \delta(E - E_F) d\mathbf{k}$ (atomic units) in the fictitious nonmagnetic state.

Element	In-plane	c-axis
Gd	0.679	1.247
Tb	0.655	1.257
Dy	0.609	1.217
Ho	0.571	1.166
Er	0.548	1.135
Tm	0.532	1.108

Er, and 3.74 (2.16) for Tm. The worst agreement is found for Gd, Tb, and especially Tm. Similar disagreement is, of course, found for polycrystals. This systematic underestimation suggests that while the electronic structure is likely described reasonably well, the scattering *rates* are in reality much higher than predicted by our classical frozen-spin-disorder model.

We have verified the reliability of our description of the electronic structure by comparing the electronic bands of Gd to highly precise full-potential calculations and found that a slightly improved treatment with added empty spheres does not materially change the results (see Appendix B for details). We have also checked the effect of including the $4f$ states in the basis set using the LDA + U method, as described in Sec. II A, using Gd and Ho as representative examples. As shown in Fig. 3, the SDR values obtained in this way for both Gd and Ho are enhanced compared to the open-core approximation, but the majority of this enhancement is due to the larger exchange splitting in the LDA + U calculation. (This effect is likely due to the dependence of the f-d exchange integral on the energy of the $4f$ wave function.) There is also a small enhancement of about 5% due to the use of a collinear Ising-like random distribution instead of a fully noncollinear random distribution. After accounting for these contributions, we find that the remaining effect of including the $4f$ states in the basis set is an SDR enhancement in the range of 12–20%. According to photoemission data,[31] the $4f$ states of other heavy rare-earth elements also lie far from the Fermi level compared to the exchange splitting and therefore should not strongly affect spin-disorder scattering.

As discussed in Sec. I, the localized character of the $4f$ states suggests that their quantum character needs to be taken into account. In two simple models assuming either very strong or very weak S-L coupling in the fully localized $4f$ shell, the quantum correction to our classical results is either $(J+1)/J$ or $(S+1)/S$. In Ref. 10, it was argued that all experimental results agree with the strong-coupling $(J+1)/J$ correction, but only after an empirical electronic correction was introduced. Since in our calculations all electronic structure effects are *already* included, we can see whether a quantum correction can systematically improve agreement with experiment without any additional adjustable parameters. The results predicted by two kinds of quantum corrections are included in Fig. 4.

Both correction factors are always greater than 1, and therefore they tend to improve the agreement with experiment. It is clear, however, that the $(J+1)/J$ correction is generally insignificant. The $(S+1)/S$ correction provides a much more notable improvement, particularly for Ho and Er, and to a lesser degree for other elements. However, the disagreement for Gd and Tb remains significant, particularly considering that the results shown in Fig. 4 are based on the atomic potentials taken from the ferromagnetic state. Therefore, it is likely that the $(S+1)/S$ correction does not fully capture the effects of the quantum character of the $4f$ shell on conduction electron scattering.

Full-potential band structure calculations show that the conduction-band structure is quite insensitive to the orbital structure of the $4f$ shell, as long as its total spin is kept fixed (see Appendix C). Therefore, the random multipole potential generated by the (hypothetical) fluctuations of the orbital structure of the $4f$ shell does not provide an important scattering mechanism. Nevertheless, these fluctuations can affect the scattering rates by modifying the allowable sets of initial and final states for electron scattering.

Apart from more complicated quantum corrections, two other mechanisms can further enhance SDR. First, we found that the inclusion of spin-orbit coupling for conduction electrons in DLM increases the resulting SDR of Gd by approximately 20% for both transport directions, and for both ferromagnetic and DLM values of the local moments. Second, the assumption that phonon and spin-disorder scattering mechanisms are entirely independent and contribute additively to the total resistivity may be wrong. If deviations from Matthiessen's rule for phonon and spin-disorder mechanisms are important, then they should be more pronounced in Gd and Tb where the Curie temperature is large and comparable with the Debye temperature. This issue deserves a separate study, which is beyond the scope of the present paper.

VI. CONCLUSIONS

In this paper, we investigated the SDR of the heavy rare-earth metals using two complementary approaches, one based on the explicit spin-disorder averaging of the Landauer-Büttiker conductance of a supercell, and another one using linear response calculations in the paramagnetic state described by the coherent potential approximation (DLM method). The two methods agree well with each other and properly capture the crystallographic anisotropy of the spin-disorder resistivity. A fairly universal linear $\rho(\Delta^2)$ dependence is obtained for the series, where Δ is the exchange splitting of the conduction band in the ferromagnetic state.

The calculated spin-disorder resistivities are systematically smaller than experiment, suggesting that the scattering rates are underestimated by the classical frozen-spin-disorder model. A quantum correction factor of $(S+1)/S$ significantly improves the agreement with experiment, especially for heavier elements. Moderate improvement is also obtained in individual cases by including the $4f$ states in the basis set and by including spin-orbit coupling. Still, all of these corrections are insufficient, at least for Gd and Tb. Since in these two elements the Curie and Debye temperatures are comparable, it is possible that deviations from Matthiessen's rule for spin-disorder and phonon scattering may be important.

ACKNOWLEDGMENTS

We thank A. L. Wysocki for useful discussions. The work at UNL was supported by the NSF through Grant No. DMR-1005642 and Nebraska MRSEC (Grant No. DMR-0820521), and completed utilizing the Holland Computing Center at the University of Nebraska. K.D.B. acknowledges financial support from the Research Corporation through the Cottrell Scholar Award. J.K., V.D., and I.T. thank the Czech Science Foundation (Grant No. P204/11/1228), and S.K. the Austrian FWF (SFB ViCoM F4109-N13), for financial support.

APPENDIX A: CONVERGENCE WITH RESPECT TO SUPERCELL CROSS SECTION

The cross section of the supercells used in the LB calculations was chosen to be large enough to minimize finite-size

TABLE III. The dependence of the SDR on the supercell cross section (units of $\mu\Omega$ cm).

	in-plane		c-axis	
Element	(3 × 2)	(4 × 3)	(4 × 4)	(5 × 5)
Gd (7.72 μ_B)			44.9	43.8
Ho (4.20 μ_B)	16.7	16.5	8.4	8.6
Tm (2.21 μ_B)	5.96	6.05	3.43	3.55
Tm (2.088 μ_B)	3.00	3.09	1.67	1.71

effects. The sufficiency of these sizes was established by convergence tests for Gd, Ho, and Tm. For c-axis transport, we increased the cross section to 5×5 (area of $12.5a^2\sqrt{3}$ with 25 atoms per monolayer) and integrated using a 20×20 k-point mesh. For in-plane transport, we increased the cross section to 4×3 (area of $12ac\sqrt{3}$ with 24 atoms per monolayer) and integrated using a 12×12 k-point mesh.

Table III summarizes the dependence of the SDR on the supercell cross section. The local moment used for each element is included in the table. We used the reduced moment taken from DLM for Ho, and both the ferromagnetic and DLM local moments for Tm. The results for different cross sections agree very well in all cases.

APPENDIX B: COMPARISON WITH FULL-POTENTIAL BAND STRUCTURE

To verify the adequacy of our TB-LMTO representation of the band structure, we chose Gd as a representative example and performed a full-potential linearized augmented plane wave (FLAPW) calculation using the FLEUR software package[41] for comparison. The $4f$ states were kept in the partially polarized core, as in most of the TB-LMTO calculations reported here. The FLAPW and LMTO band structures for Gd are shown in Fig. 5(a). Our FLAPW calculation is consistent with the one reported in Ref. 30 and fits well with angle-resolved photoelectron spectroscopy measurements.[42] Near the Fermi level, the TB-LMTO band structure is quite close to FLAPW, but there is a notable deviation along the H-K and K-Γ symmetry lines.

The agreement with the FLAPW band structure is improved by adding empty spheres in the TB-LMTO basis set. We included the unoccupied $5f$ orbitals in the basis set for Gd and reduced the local Gd moment to 7.603 μ_B using FSM. The resulting band structure is shown in Fig. 5(b); the agreement with FLAPW near the Fermi level is now almost perfect.

The SDR was calculated in the same way as described in Sec. II A with the following modifications: the c axis is calculated using a 2×2 supercell with 4 Gd atoms per monolayer (there are 12 empty spheres surrounding each monolayer of 4 Gd atoms); random spin disorder is introduced only on the Gd sites; 48×48 k-point mesh is used for Brillouin-zone integration; and the conductance for each thickness is configurationally averaged over 30 random spin configurations.

The calculated SDR using the adjusted band structure is 47.4 $\mu\Omega$ cm, which is 6% larger than the result of 44.9 $\mu\Omega$ cm reported in Table I. This increase is not statistically significant. Therefore, we conclude that the original TB-LMTO representation of the band structure is sufficiently accurate for SDR calculations.

APPENDIX C: FLUCTUATIONS OF THE ORBITAL STRUCTURE OF THE $4f$ SHELL

The effect on the conduction bands of the multipole potential generated by variations in the orbital structure of

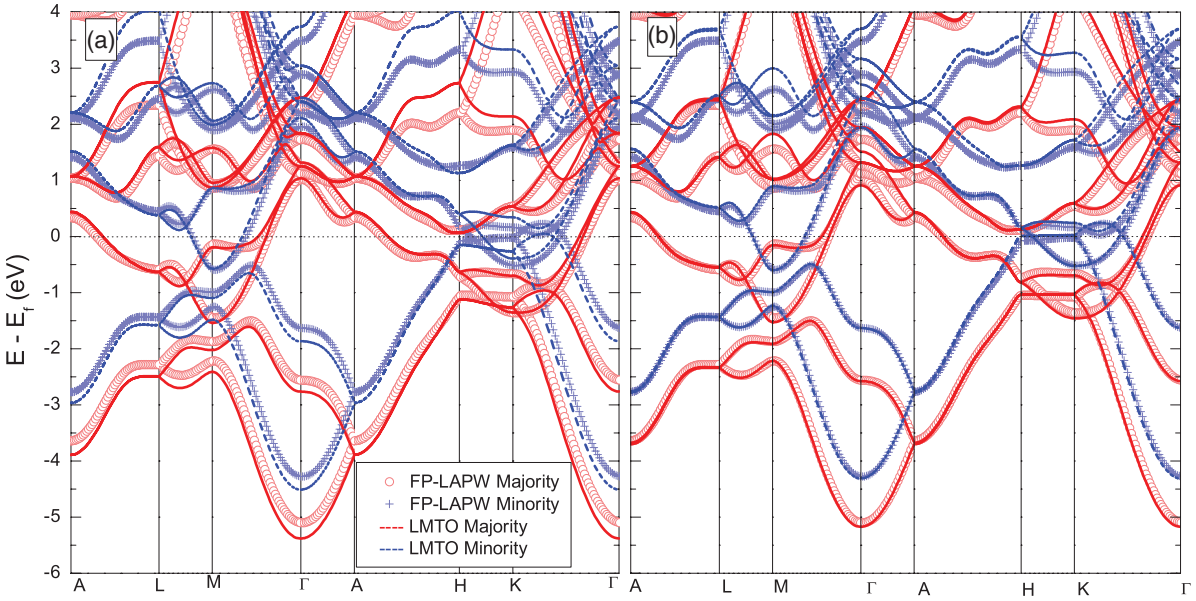

FIG. 5. (Color online) Band structures calculated using TB-LMTO and full-potential linear augmented plane wave (FLAPW) methods. Solid red line: majority-spin LMTO; dashed blue line: minority-spin LMTO. Open red circles: majority-spin FLAPW; blue plus signs: minority-spin FLAPW. (a) No empty spheres in the LMTO basis set. (b) With empty spheres in the LMTO basis set. Note the improved agreement along the H-K and K-Γ symmetry lines.

the $4f$ states (violating Hund's rules) was evaluated using a FLAPW[41] calculation for Ho. For this purpose, the $4f$ states were included in the valence basis and subjected to the LDA + U potential (fully localized limit[34] with $U = 7.5$ eV and $J = 0.7$ eV). The band structures for different orbital occupations of the $4f$ shell corresponding to orbital momenta $L = 0, 4, 5$, and 6 were calculated self-consistently. We found no detectable effect of the $4f$ shell orbital structure on the conduction bands near the Fermi energy; the bands were modified only close to the unoccupied $4f$ states, which in all cases were more than 1 eV above the Fermi energy. Therefore, we conclude that fluctuations of the orbital structure of the $4f$ shell do not materially contribute to the scattering potential seen by the conduction electrons.

[1] B. R. Coles, Adv. Phys. **7**, 40 (1958).
[2] N. F. Mott, Adv. Phys. **13**, 325 (1964).
[3] S. V. Vonsovskii, *Magnetism* (Halsted, New York, 1974).
[4] T. Moriya, *Spin Fluctuations in Itinerant Electron Magnetism* (Springer, Berlin, 1985).
[5] T. Kasuya, Prog. Theor. Phys. **16**, 58 (1956).
[6] T. Kasuya, Prog. Theor. Phys. **22**, 227 (1959).
[7] A. J. Dekker, J. Appl. Phys. **36**, 906 (1965).
[8] K. N. R. Taylor and M. I. Darby, *Physics of Rare Earth Solids* (Chapman and Hall, London, 1972).
[9] B. Coqblin, *The Electronic Structure of Rare-earth Metals and Alloys: The Magnetic Heavy Rare-earths* (Academic, New York, 1977).
[10] S. Legvold, Phys. Rev. B **3**, 1640 (1971).
[11] H. Miwa, Prog. Theor. Phys. **28**, 208 (1962).
[12] A. R. Mackintosh, Phys. Rev. Lett. **9**, 90 (1962).
[13] R. J. Elliott and F. A. Wedgwood, Proc. Phys. Soc. **81**, 846 (1963).
[14] A. L. Wysocki, R. F. Sabirianov, M. van Schilfgaarde, and K. D. Belashchenko, Phys. Rev. B **80**, 224423 (2009).
[15] B. L. Gyorffy, A. J. Pindor, J. Staunton, G. M. Stocks, and H. Winter, J. Phys. F: Met. Phys. **15**, 1337 (1985).
[16] S. Legvold, F. H. Spedding, F. Barson, and J. F. Elliott, Rev. Mod. Phys. **25**, 129 (1953).
[17] R. V. Colvin, S. Legvold, and F. H. Spedding, Phys. Rev. **120**, 741 (1960).
[18] P. M. Hall, S. Legvold, and F. H. Spedding, Phys. Rev. **117**, 971 (1960).
[19] R. W. Green, S. Legvold, and F. H. Spedding, Phys. Rev. **122**, 827 (1961).
[20] D. L. Strandburg, S. Legvold, and F. H. Spedding, Phys. Rev. **127**, 2046 (1962).
[21] D. E. Hegland, S. Legvold, and F. H. Spedding, Phys. Rev. **158**, 158 (1963).
[22] H. E. Nigh, S. Legvold, and F. H. Spedding, Phys. Rev. **132**, 1092 (1963).
[23] L. R. Edwards and S. Legvold, Phys. Rev. **176**, 753 (1968).
[24] M. D. Wilding and E. W. Lee, Proc. Phys. Soc. **85**, 955 (1965).
[25] P. Jacobsson and B. Sundqvist, Phys. Rev. B **40**, 9541 (1989).
[26] K. Maezawa, K. Mori, K. Sato, Y. Saito, and S. Wakabayashi, J. Phys. Soc. Jpn. **43**, 1815 (1977).
[27] M. Ellerby, K. A. McEwen, and J. Jensen, Phys. Rev. B **57**, 8416 (1998).
[28] M. Ellerby, K. A. McEwen, E. Bauer, R. Hauser, and J. Jensen, Phys. Rev. B **61**, 6790 (2000).
[29] R. Brout and H. Suhl, Phys. Rev. Lett. **2**, 387 (1959).
[30] P. Kurz, G. Bihlmayer, and S. Blügel, J. Phys. Condens. Matter **14**, 6353 (2002).
[31] Y. Baer and W.-D. Schneider, in *Handbook on the Physics and Chemistry of Rare Earths*, edited by K. A. Gschneidner Jr., L. Eyring, and S. Hfner, Vol. 10 (North-Holland Physics, Amsterdam, 1987), pp. 1–73.
[32] O. K. Andersen, Phys. Rev. B **12**, 3060 (1975).
[33] I. Turek, J. Kudrnovský, G. Bihlmayer, and S. Blügel, J. Phys. Condens. Matter **15**, 2771 (2003).
[34] A. I. Liechtenstein, V. I. Anisimov, and J. Zaanen, Phys. Rev. B **52**, R5467 (1995).
[35] A. Burusz, L. Szunyogh, and P. Weinberger, Philos. Mag. **88**, 2615 (2008).
[36] I. Turek, J. Kudrnovský, V. Drchal, L. Szunyogh, and P. Weinberger, Phys. Rev. B **65**, 125101 (2002).
[37] K. Carva, I. Turek, J. Kudrnovský, and O. Bengone, Phys. Rev. B **73**, 144421 (2006).
[38] S. Khmelevskyi, I. Turek, and P. Mohn, Phys. Rev. B **70**, 132401 (2004).
[39] J. K. Alstad, R. V. Colvin, and S. Legvold, Phys. Rev. **123**, 418 (1961).
[40] I. Turek, V. Drchal, J. Kudrnovský, M. Sob, and P. Weinberger, *Electronic Structure of Disordered Alloys, Surfaces and Interfaces* (Kluwer Academic, Boston, 1997).
[41] S. Blügel and G. Bihlmayer, in *Computational Nanoscience: Do It Yourself!*, edited by J. Grotendorst, S. Blügel, and D. Marx, NIC Series Vol. 31 (John von Neumann Institute for Computing, Jülich, 2006), p. 85; [www.flapw.de].
[42] K. M. Döbrich, A. Bostwick, E. Rotenberg, and G. Kaindl, Phys. Rev. B **81**, 012401 (2010).